

Wind tunnel testing of wind turbine and wind farm control strategies for active power regulation

Gonzalez Silva, J.; van der Hoek, D.; Ferrari, R.; van Wingerden, J. W.

DOI

[10.1063/5.0215493](https://doi.org/10.1063/5.0215493)

Publication date

2024

Document Version

Final published version

Published in

Journal of renewable and sustainable energy

Citation (APA)

Gonzalez Silva, J., van der Hoek, D., Ferrari, R., & van Wingerden, J. W. (2024). Wind tunnel testing of wind turbine and wind farm control strategies for active power regulation. *Journal of renewable and sustainable energy*, 16(5), Article 053302. <https://doi.org/10.1063/5.0215493>

Important note

To cite this publication, please use the final published version (if applicable). Please check the document version above.

Copyright

Other than for strictly personal use, it is not permitted to download, forward or distribute the text or part of it, without the consent of the author(s) and/or copyright holder(s), unless the work is under an open content license such as Creative Commons.

Takedown policy

Please contact us and provide details if you believe this document breaches copyrights. We will remove access to the work immediately and investigate your claim.

RESEARCH ARTICLE | SEPTEMBER 06 2024

Wind tunnel testing of wind turbine and wind farm control strategies for active power regulation

Special Collection: [Wind Tunnel Research for Renewable Energies](#)

J. Gonzalez Silva   ; D. van der Hoek  ; R. Ferrari  ; J. W. van Wingerden 

 Check for updates

J. Renewable Sustainable Energy 16, 053302 (2024)

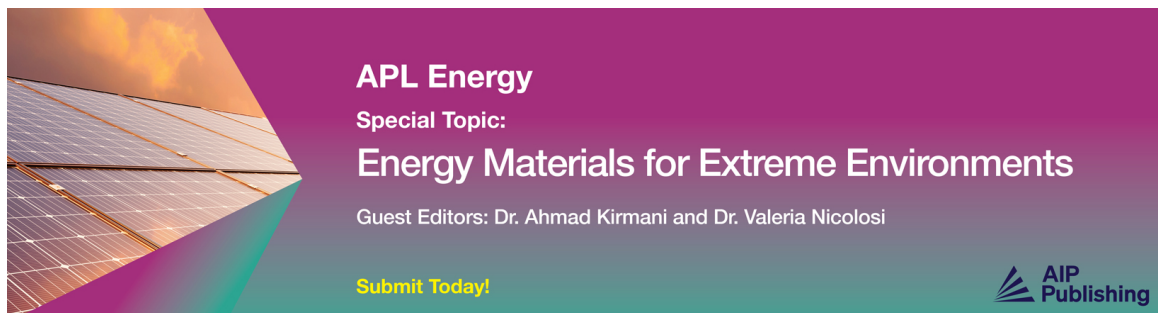
<https://doi.org/10.1063/5.0215493>



View
Online




Export
Citation



APL Energy
Special Topic:
Energy Materials for Extreme Environments
Guest Editors: Dr. Ahmad Kirmani and Dr. Valeria Nicolosi

[Submit Today!](#)

 AIP
Publishing

Wind tunnel testing of wind turbine and wind farm control strategies for active power regulation

Cite as: J. Renewable Sustainable Energy **16**, 053302 (2024); doi: 10.1063/5.0215493

Submitted: 24 April 2024 · Accepted: 21 August 2024 ·

Published Online: 6 September 2024



View Online



Export Citation



CrossMark

J. Gonzalez Silva,^{a)}  D. van der Hoek,  R. Ferrari,  and J. W. van Wingerden 

AFFILIATIONS

Delft Center of Systems and Control, Faculty of Mechanical Engineering, Delft University of Technology, Delft, The Netherlands

Note: This paper is part of the Special Topic on: Wind Tunnel Research for Renewable Energies.

^{a)} Author to whom correspondence should be addressed: J.GonzalezSilva@tudelft.nl

ABSTRACT

Wind energy has emerged as a prominent alternative energy source, harvesting energy through turbines to contribute sustainably to the electricity grid. Effective control of these turbines is crucial for regulating power generation, with wind farm control strategies geared toward maximizing on-demand energy generation. In this work, we propose a wind turbine regulator based on blade-pitch actuation and assess the impact of adopted turbine derating strategies on aerodynamic loading and downstream power availability in an experimental setting. By considering a derating strategy based on generator torque control law, we explore two wind farm control approaches: thrust balance and power compensation. Our findings highlight the advantages of balancing aerodynamic loads across the farm, preventing turbine saturation, and enhancing power availability by 3%–5% compared to a uniform power dispatch. Furthermore, the inclusion of power compensation results in a heightened upper limit in wind farm power tracking, indicating a 22% boost in wind farm power availability. This research underscores the potential benefits of innovative turbine regulation strategies for optimizing wind farm performance and enhancing overall energy flexibility.

© 2024 Author(s). All article content, except where otherwise noted, is licensed under a Creative Commons Attribution-NonCommercial-NoDerivs 4.0 International (CC BY-NC-ND) license (<https://creativecommons.org/licenses/by-nc-nd/4.0/>). <https://doi.org/10.1063/5.0215493>

I. INTRODUCTION

Current wind turbines usually operate to maximize their own power generation. When placing them together, the deployment cost and the amount of area needed for usage are reduced. However, a notable challenge arises from the interactions between turbines induced by their wakes¹—the turbulent downstream wind structures created by the energy extraction from the rotor blades. The conventional operation of wind turbines, neglecting each turbine's impact on other turbines through its wake, is considered a greedy approach. Strategies such as axial induction and wake steering control have been proposed in the literature to address the issue of wake interactions.² Recently, wake-mixing techniques have been suggested that apply a sinusoidal thrust excitation to enhance wake recovery.³ The emphasis on maximizing power generation is predominantly employed because wind energy constitutes a small share of the total power generation, with other energy sources typically taking over the grid regulation.

As the share of wind energy grows, the maximization paradigm is expected to shift to a demand–response source. To supply sufficient stability throughout the electrical grid, wind farms would instead regulate their power generation to the demand.^{4–6} Such a transformation is

beneficial for the future of wind energy. Yet, insufficient wind may still render the grid susceptible to system splits, blackouts, and instabilities. Therefore, discussions to address power system stability challenges due to the variability of wind sources are gathering momentum.^{7,8} To overcome these challenges, for instance, storage units have been proposed as presented by Morales *et al.*,⁹ including batteries and hydrogen plants. Moreover, the integration with other energy sources that present flexible power regulation capabilities, such as hydropower, solar power, and nuclear energy, has been recommended.^{10–12} While energy integration efforts are crucial for the future, in this work, we focus on wind farm control techniques to provide more flexible and reliable wind energy solutions from the wind power plants themselves. Through wind tunnel testing, we explored the on-demand power tracking capability of single turbines and their collaboration within a farm.

To enhance wind energy flexibility, requirements have been placed to equip wind turbines with derating capabilities.¹³ This aims to improve the integration of wind energy into the grid. With the increasing penetration of wind energy, it is important for wind farms to actively contribute to frequency regulation, i.e., providing active power

control (APC) services to the grid. In the existing literature, different derating control strategies have been proposed.^{14–16} Aho *et al.*¹⁴ presented two derating approaches: APC torque control and APC pitch control. The APC torque control maintains a high rotor speed, which is favorable for power regulation since energy is stored as kinetic energy by the rotating components. This kinetic energy enables greater responsiveness to rapid changes in power demand. On the other hand, lowering rotor speed, with the APC pitch control, leads to improved lower structural loads, as demonstrated by van der Hoek *et al.*¹⁵ It is important to note that there is an infinite number of operating conditions that can achieve a desired down-regulation, a point underscored by Lio *et al.*¹⁶ The wind flow and the interaction between turbines vary based on the adopted derating control strategy. In the works of Ma *et al.*¹⁷ and Kim *et al.*,¹⁸ lower rotor speed methods are suggested in a wind farm context because they result in lower thrust forces, reducing the wind deficit and consequently benefiting downstream turbines. Ideally, derating while considering a minimum thrust force would maximize wind farm power availability. However, this approach relies heavily on accurate wind speed estimates, which are challenging to obtain in highly waked scenarios. This reliance often leads to degraded performance¹⁹ and can result in shutdowns at lower rotor speeds. Here, we derive and investigate a low rotor speed approach similar to APC pitch control that does not directly use the wind speed information in the controller, overcoming the challenges of the minimum thrust force method.

Wind farm control considering aerodynamic loads is in the early stages. The concept was presented and assessed by simulations in Vali *et al.*²⁰ and Silva *et al.*,²¹ where the contributions of individual turbines to the total power output are modified online through feedback based on the turbines' structural loading. Taking into account thrust forces can not only reduce the wind deficit but also avoid the overloading of specific turbines due to prevailing wind conditions, thereby reducing sporadic failures and consequently maintenance costs. These are promising outcomes, especially within the offshore wind sector. In offshore sites, the access for maintenance operations is limited and the turbines are placed in a highly corrosive environment that accelerates degradation and amplifies fatigue, thereby increasing failure rates.²²

Regarding wind farm power regulation, a fundamental approach involves employing a balanced and equitable power generation across turbines.²³ This strategy entails derating all turbines equally to meet an overall demand lower than the wind farm's capacity. Each turbine receives an equal share of the total power demand, aiming to prevent overloading of any particular turbine, irrespective of wake interactions. However, uniform power generation may result in uneven power availability due to the wake effects, potentially leading to turbine *saturation*, where turbines fail to meet demands that surpass their maximum available power capacity. In such scenarios, as a remedy, turbines with available power can increase power generation and compensate for others with insufficient power availability. A real-time closed-loop solution, introduced by van Wingerden *et al.*²⁴ using a simple but effective PI controller, shows through simulations to enhance wind farm power output by alleviating power fluctuations. In Silva *et al.*,^{21,25} the authors extended this approach to assess power losses due to turbine *saturation* and implemented it concurrently with the thrust force balancing in simulations. The real-time feedback approach contrasts with typical axial induction control approaches, which rely on steady-state models and lookup tables to maximize

power and have demonstrated limited benefits in realistic conditions.^{26,27}

This paper contributes by deriving derating control strategies and elucidating their impact from a wind farm perspective through wind tunnel testing. Additionally, it validates wind farm control strategies, particularly real-time feedback controllers for thrust force balancing and power compensation in the presence of turbine *saturation*, transitioning from numerical simulations to experimental setups. Previous experimental works, such as those by Campagnolo *et al.*,²⁸ focused on power maximization. Furthermore, Petrović *et al.*²⁹ performed experiments with a closed-loop wind farm controller for APC but did not evaluate turbine saturation scenarios nor account for loads.

The remainder of this paper is structured as follows: The experiments are conducted with scaled wind turbines in the wind tunnel, described in Sec. II. The considered derating control strategies are presented in Sec. III. The wind farm controller, which compensates for power and balances loads in the farm, is described in Sec. IV. The results are reported in Sec. V, where we first demonstrate the effects of different derating control strategies on a single turbine and in a wind farm setting in Sec. V A. Next, we evaluate the effectiveness of thrust force balancing to showcase the reduction of fatigue loads and the enhancement of wind farm power availability in Secs. V B and V C, respectively. Then, we assess the effectiveness of power compensation in the presence of turbine saturation in Sec. V D. Finally, the conclusions are presented in Sec. VI.

II. EXPERIMENTAL SETUP

The experiments were performed in a novel modular wind tunnel at the Delft University of Technology. The wind tunnel was tailored to replicate diverse wind conditions, prioritizing practicality through modular compartments. The wind tunnel consists of a WindShape unit³⁰ with a square outlet of $2.1 \times 2.1 \text{ m}^2$, typically utilized for drone testing. The WindShape is composed of 9×9 modules, each containing nine pairs of counter-rotating computer fans, which allow personalizing the desired wind profile, with a maximum wind speed of 15 m/s. Additionally, the wind tunnel includes modular compartments that contain the flow for a desired length. The scaled wind turbines are placed in specific modular compartments, defining their distancing. An overview of the experimental setup is provided in Fig. 1.

For the experiments, we utilized three MoWiTo-0.6 wind turbines developed by the University of Oldenburg.³¹ This three-bladed, horizontal-axis wind turbine has a rotor diameter of $D = 0.58 \text{ m}$ and is equipped with a generator that allows torque control and a stepper motor for collectively pitching blades. The base of the turbine tower is equipped with a set of strain gauges in a full Wheatstone bridge to measure the tower bending moment.

The wall interference from the tunnel compartments can be considered negligible,³² where the blockage effect, defined as the ratio of the rotor-swept area divided by the wind tunnel cross-sectional area, is 6%. The hub center of the turbines was $0.672D$ above the tunnel floor. Hence, interference effects from the ground are about as expected at full scale. The three wind turbines are spaced $3.9D$ apart to operate in full wake conditions. Only the full wake condition is considered because it represents the worst-case scenario regarding power availability. The tests were conducted at constant inflow velocities at 7 and 8 m/s with an inherent turbulence intensity of $TI \approx 4\%$, and no vertical wind profile.

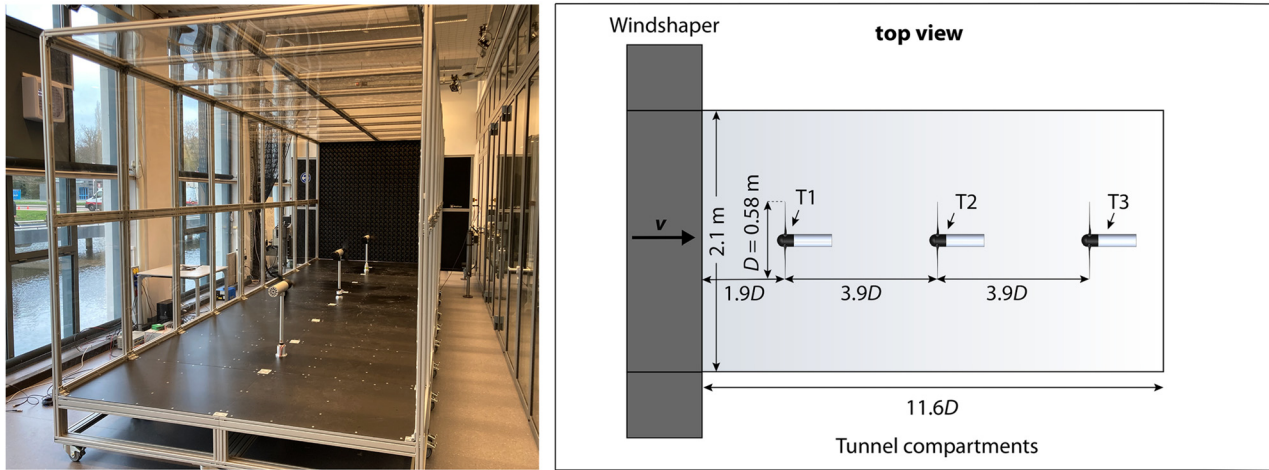


FIG. 1. Illustrations of the experimental setup: photo of the wind tunnel and the three scaled turbines in operation on the right; and the layout details on the left.

The control system is established as illustrated in Fig. 2. Communication between the wind turbines and the computer is arranged with a dSPACE *MicroLabBox*. The dSPACE *MicroLabBox* offers a real-time interface with MATLAB's Simulink® through dSPACE *ControlDesk* software. The controllers for the wind turbines and the wind farm, as well as the estimators for wind speed and thrust, are developed in MATLAB's Simulink® and compiled to run within dSPACE *ControlDesk* at a frequency of 2 kHz. The recorded signals from the turbines encompass rotor speed, pitch angles, generator torque, and strain at the tower base. These signals are utilized in the controllers and estimators. The actuator signals include the generator torque and blade-pitch angles; yaw control is not considered in the scope of this work. Aiming to investigate control algorithms in an experimental setup, this setup has also been used to explore wake-mixing strategies.³³

III. DERATING CONTROL STRATEGIES

Control strategies utilizing blade pitching for derating purposes have been demonstrated as beneficial for wind farms, not only in terms of reducing structural loading but also in enhancing wind farm power availability.^{17,18} The advantage in terms of wind farm power generation lies in the significant reduction of wind deficit achieved through blade pitching, as opposed to relying solely on pure generator torque control for derating. This reduction of wind deficit behind the derated turbine is particularly beneficial for downstream turbines, enhancing overall wind farm power availability. Consequently, our focus is on derating strategies that utilize blade pitching.

The definition of a derating strategy involves establishing a framework for determining the blade pitching strategy, consequently affecting the generator torque through changes in the rotor speed. First, we formulate the closed-loop controller that regulates the rotor speed based on blade pitching in Sec. III A. Different definitions of the

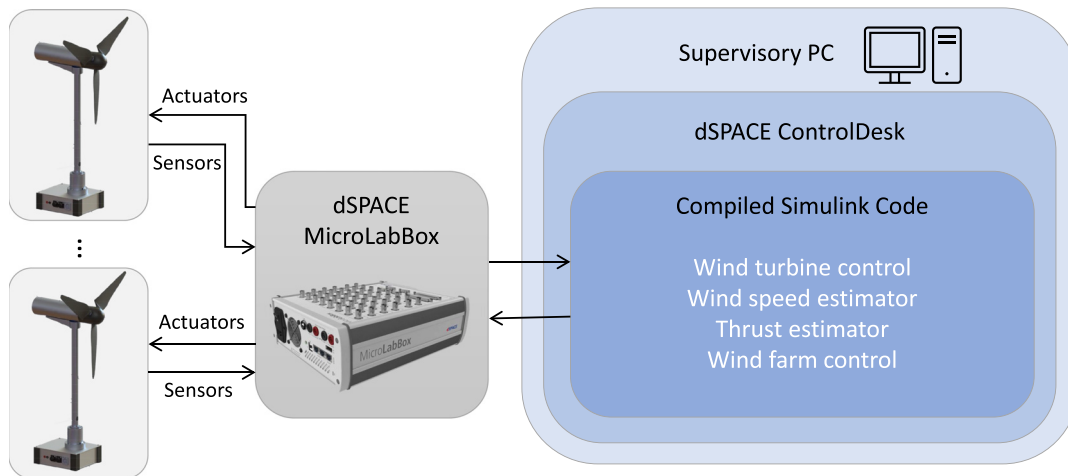


FIG. 2. Control structure utilizing real-time interface with dSPACE and Simulink.

reference rotor speeds lead to different operating conditions, i.e., combinations of blade pitching and generator torque, that result in distinct turbine performances and wake characteristics. As a result, we propose and evaluate two strategies: (1) derating control by blade pitching based on the greedy generator torque control, presented in Sec. III B, and (2) derating control by blade pitching with constant tip speed ratio, in Sec. III C.

A. Blade-pitch controller for derating strategies

The main goal of the blade-pitch controller is to regulate the rotor speed to a desired set-point by pitching the blades. To obtain the blade-pitch controller for the derating control strategies, we follow the derivation of the baseline blade-pitch control utilized in the above-rated wind speed conditions from Hansen *et al.*³⁴ and Butterfield *et al.*³⁵ The blade-pitch controller is designed using the drive-train model defined as

$$T_{\text{aero}} - G_b T_{\text{gen}} = J_{\text{LSS}} \Delta \dot{\omega}_r, \quad (1)$$

where T_{aero} is the low-speed shaft aerodynamic torque, T_{gen} is the high-speed shaft generator torque, G_b is the high-speed to low-speed gearbox ratio, J_{LSS} is the rotational components' equivalent inertia, corresponding to the low-speed shaft, $\Delta \dot{\omega}_r$ is the low-speed shaft rotational acceleration. The generator torque T_{gen} can be configured in two ways. First, it can be adjusted to match the specified reference power P^{ref} . In that case, it exhibits an inverse relationship with the generator speed and is referred to as a *tracking* mode. Alternatively, the generator torque can be set to maximize power extraction, operating in a mode known as *greedy*. This mode is reached when the turbine cannot meet the power demand, so it maximizes the power extraction instead. Therefore, the torque is set as

$$T_{\text{gen}} = \begin{cases} T_{\text{gen,tracking}}(P^{\text{ref}}, \omega_r) = \frac{P^{\text{ref}}}{G_b \omega_r} & \text{if in tracking mode;} \\ T_{\text{gen,greedy}}(\omega_r) = K_{\text{gen}} \omega_r^2 & \text{else if in greedy mode.} \end{cases} \quad (2)$$

Here, K_{gen} is the greedy generator torque gain based on the steady-state aerodynamics, and ω_r is the low-speed shaft rotational velocity. Conversely, the aerodynamic torque is dependent not only upon the rotor speed but also on the blade-pitch angles and wind speed, as expressed in the following equation:

$$T_{\text{aero}}(\theta, \omega_r, v) = \frac{P(\theta, \omega_r, v)}{\omega_r}, \quad (3)$$

where P is the mechanical power, θ is the collective blade-pitch angle, and v is the inflow wind speed.

Taking the first-order Taylor series expansion of the above expressions, we have

$$T_{\text{gen,tracking}}(P^{\text{ref}}, \omega_r) \approx \frac{P_0^{\text{ref}}}{G_b \omega_{r,0}} - \frac{P_0^{\text{ref}}}{G_b \omega_{r,0}^2} \Delta \omega_r + \frac{1}{G_b \omega_{r,0}} \Delta P^{\text{ref}}, \quad (4)$$

$$T_{\text{gen,greedy}}(\omega_r) \approx K_{\text{gen}} \omega_{r,0}^2 + 2K_{\text{gen}} \omega_{r,0} \Delta \omega_r, \quad (5)$$

and

$$T_{\text{aero}}(\theta, \omega_r, v) \approx \frac{P_0}{\omega_{r,0}} + \frac{1}{\omega_{r,0}} \frac{\partial P}{\partial \theta} \Big|_0 \Delta \theta + \frac{1}{\omega_{r,0}} \frac{\partial P}{\partial \omega_r} \Big|_0 \Delta \omega_r - \frac{P_0}{\omega_{r,0}^2} \Delta \omega_r + \frac{1}{\omega_{r,0}} \frac{\partial P}{\partial v} \Big|_0 \Delta v, \quad (6)$$

where $\Delta \omega_r$, ΔP^{ref} , $\Delta \theta$, and Δv are small perturbations from the operation point 0 of the low-speed shaft rotational speed, the reference power, the collective blade-pitch angle, and the inflow wind speed, respectively. $\frac{\partial P}{\partial \theta}$, $\frac{\partial P}{\partial \omega_r}$, and $\frac{\partial P}{\partial v}$ are the sensitivity of aerodynamic power to collective blade-pitch angle, to the rotor speed, and to the inflow wind speed, respectively. The terms of the aerodynamic torque associated with the perturbations of the low-speed shaft rotation speed and the inflow wind speed are expected to be approximately three orders of magnitude lower than the term associated with the perturbation of collective blade-pitch angle. This assessment is based on the observed rates of change—approximately 5 rad/s² for the low-speed shaft rotation speed, 1°/s for the collective blade-pitch angle, and 0.02 m/s² for the inflow wind speed—and the operational conditions, which include a low-speed shaft rotation speed of 130 rad/s, a power output of 13 W, collective blade-pitch angle at 6°, and an inflow wind speed of 8 m/s. Therefore, as a design decision, we focus on the aerodynamic torque changes with respect to the collective blade-pitch angle solely, so the aerodynamic torque is simplified, in accordance with,^{34,35} as

$$T_{\text{aero}}(\theta) \approx \frac{P_0}{\omega_{r,0}} + \frac{1}{\omega_{r,0}} \frac{\partial P}{\partial \theta} \Big|_0 \Delta \theta. \quad (7)$$

We apply a proportional-integral-derivative (PID) control law to dynamically adjust the collective blade-pitch angle based on the rotor speed perturbation, acting as the reference error. This strategy ensures precise rotor speed regulation while tracking the desired power set-point. The variation in the collective blade-pitch angle is defined as

$$\Delta \theta = K_P G_b \Delta \omega_r + K_I \int_0^t G_b \Delta \omega_r dt + K_D G_b \Delta \dot{\omega}_r, \quad (8)$$

where K_P , K_I , and K_D are the blade-pitch controller proportional, integral, and derivative gains, respectively. If the applied generator torque corresponds to the tracking generator torque outlined in Eq. (4), combining with Eqs. (1), (7), and (8), the equation of motion for the rotor speed error can be derived as

$$\underbrace{\left[J_{\text{LSS}} + \frac{1}{\omega_{r,0}} \left(-\frac{\partial P}{\partial \theta} \Big|_0 \right) K_D G_b \right]}_M \Delta \ddot{\omega}_r + \underbrace{\left[\frac{1}{\omega_{r,0}} \left(-\frac{\partial P}{\partial \theta} \Big|_0 \right) K_P G_b - \frac{P_0^{\text{ref}}}{\omega_{r,0}^2} \right]}_C \Delta \dot{\omega}_r + \underbrace{\frac{1}{\omega_{r,0}} \left(-\frac{\partial P}{\partial \theta} \Big|_0 \right) K_I G_b}_K \Delta \omega_r = -\frac{1}{\omega_{r,0}} \Delta \dot{P}^{\text{ref}}. \quad (9)$$

On the other hand, if the applied generator torque matches the greedy generator torque from Eq. (5), analogously, it follows that

$$\underbrace{\left[J_{LSS} + \frac{1}{\omega_{r,0}} \left(-\frac{\partial P}{\partial \theta} \right)_0 K_D G_b \right]}_M \Delta \dot{\omega}_r + \underbrace{\left[\frac{1}{\omega_{r,0}} \left(-\frac{\partial P}{\partial \theta} \right)_0 K_P G_b + 2G_b K_{gen} \omega_{r,0} \right]}_C \Delta \dot{\omega}_r + \underbrace{\frac{1}{\omega_{r,0}} \left(-\frac{\partial P}{\partial \theta} \right)_0 K_I G_b}_{\kappa} \Delta \omega_r = 0. \quad (10)$$

To obtain the response of the rotor speed error resembling that of an idealized second-order system, the PID control with gain scheduling corresponding to the operation condition needs to be employed. A second-order system is characterized by the natural frequency, ω_n , and damping ratio, ξ . The recommended values for these parameters in controlling the scaled turbines are equal to

$$\omega_n = \sqrt{\frac{K}{M}} = 0.3 \text{ rad/s and } \xi = \frac{C}{2M\omega_n} = \frac{C\omega_n}{2K} = 0.7. \quad (11)$$

Therefore, the desired second-order system would respond to a step time with a rise time, t_r , and settling time, t_s , equal to

$$t_r = \frac{1}{\omega_n \sqrt{1 - \xi^2}} \left[\pi - \arctan \left(\frac{\sqrt{1 - \xi^2}}{\xi} \right) \right] = 10.95 \text{ s.}$$

and

$$t_s = \frac{4}{\xi \omega_n} = 19.05 \text{ s.} \quad (12)$$

To achieve these desired performance criteria, we employ the following gain scheduling:

$$K_P(\omega_r, \theta, v) = \frac{-2J_{LSS}\omega_r\xi\omega_n}{G_b \left. \frac{\partial P(\omega_r, \theta, v)}{\partial \theta} \right|_0},$$

$$K_I(\omega_r, \theta, v) = \frac{-J_{LSS}\omega_r\omega_n^2}{G_b \left. \frac{\partial P(\omega_r, \theta, v)}{\partial \theta} \right|_0}, \text{ and } K_D = 0. \quad (13)$$

The gains are scheduled with the measurements of the rotor speed and with the computed sensitivity of aerodynamic power to the collective blade-pitch angle. The measurements of the rotor speed, the current blade-pitch angle, and the wind speed information are utilized to compute the sensitivity of aerodynamic power to the collective blade-pitch angle. The derivative gain is neglected as past work indicates that it does not effectively impact the rotor speed tracking performance.³⁵ Notice that the negative damping from the tracking generator torque, $P_0^{ref}/\omega_{r,0}^2$, and the positive damping from the greedy generator torque, $2G_b K_{gen} \omega_{r,0}$, that are consolidated into the lumped damping parameter C are neglected in the gain scheduling in Eq. (13). They are neglected because transitioning between generator torque modes would result in an undesirable and non-smooth switch in K_P .

The sensitivity of aerodynamic power to the collective blade-pitch angle is computed based on the measurements of the rotor speed,

blade-pitch angles, and wind speed, utilizing the information of C_P mapping through the following relationship:

$$\frac{\partial P}{\partial \theta}(\omega_r, \theta, v) = \frac{1}{2} \rho \pi R^2 v^3 \frac{\partial C_P(\lambda, \theta)}{\partial \theta}, \quad (14)$$

where ρ is the air density, R is the rotor radius, and C_P is the power coefficient, which relates the efficiency of power extraction with the tip speed ratio $\lambda = R\omega_r/v$ and the collective blade-pitch angle θ .

This design does not include any blade-pitch actuator dynamic effects. The blade-pitch actuator dynamics are neglected because the blade-pitch actuator response is much faster than the desired pitch response from Eq. (11), with a pitch rate of approximately 30°/s. Moreover, we saturate the integration of the error in the PI controller once the minimum or the maximum blade-pitch angles are reached, as a windup prevention. The minimum blade-pitch angle is set as the fine blade-pitch angle that refers to the blade-pitch angle that jointly with the optimal generator torque maximizes power extraction.

As previously discussed, in power set-point tracking control, the choice of the reference rotor speed dictates the derating control strategy. This choice impacts the performance at both the wind turbine and wind farm levels. In this work, we assess two methodologies proposed in Subsections III B and III C.

B. Derating control strategy I: Blade pitching based on the greedy generator torque control

Adopted by Fleming *et al.*¹ and Kim *et al.*,¹⁸ and further extended to align with loading constraints in Silva *et al.*,³⁶ this methodology maps the reference power to a reference rotor speed. This relationship is established on the foundation of the greedy generator torque control law, as depicted in Fig. 3(b). To generate the map Γ , such that $\omega_r^{ref} = \Gamma(P^{ref})$, illustrated in Fig. 3(a), the associated greedy generator torque for a given rotor speed is multiplied by the rotor speed itself. In this way, the reference rotor speed correlates with the rotor speed attained when the wind speed is reduced utilizing the greedy generator torque control and fine blade-pitch angles. After determining the rotor speed through the map Γ , the blade-pitch controller derived in Sec. III A is applied, utilizing the calculated reference rotor speed. Notice that wind speed information is not required to determine the reference rotor speed, given the map Γ .

To avoid shut-downs due to the use of the tracking generator torque law, the generator torque is saturated as

$$T_{gen} = \min(T_{gen,greedy}, T_{gen,tracking}), \quad (15)$$

where $T_{gen,greedy}$ and $T_{gen,tracking}$ were previously defined in Eq. (2). This constraint will leave the power regulation to be led by the blade pitching control with a slower response when fast transients lead the tracking generator torque to high values. Furthermore, when P^{ref} is higher than the available power in the wind, i.e., the turbine reaches saturation, the blade-pitch angle meets the fine blade-pitch angle value and Eq. (15) ensures that the turbine operates at maximum energy extraction.

C. Derating control strategy II: Blade pitching with constant tip speed ratio

With this strategy, we keep the tip speed ratio constant by computing the reference rotor speed as

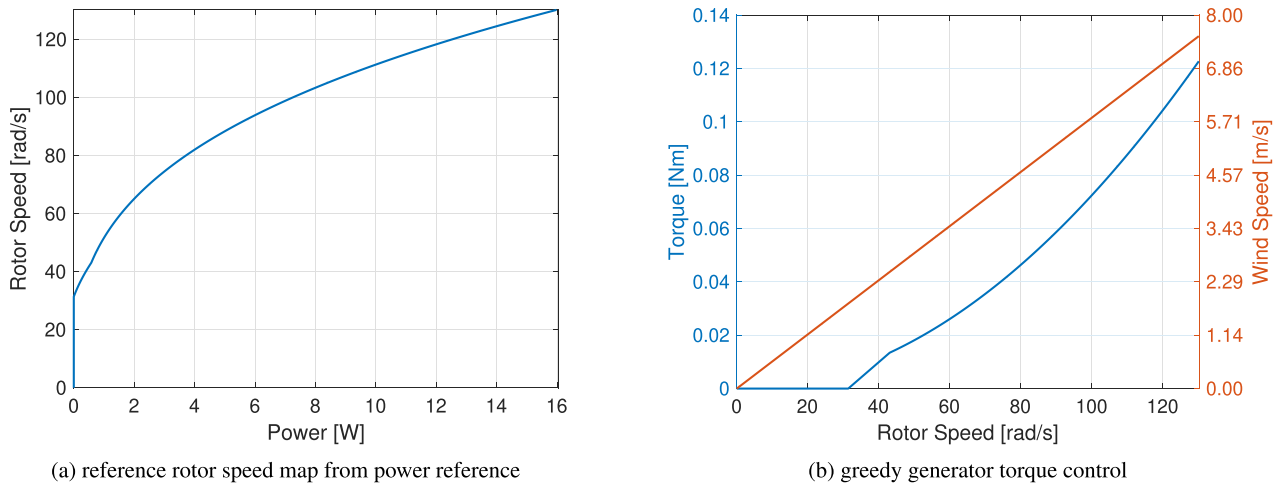


FIG. 3. Mapping from the reference power set-point to a reference rotor speed (a) based on the greedy generator torque control (b). (a) Reference rotor speed map from power reference. (b) Greedy generator torque control.

$$\omega_r^{\text{ref}} = \frac{\lambda^{\text{opt}} v}{R} \quad (16)$$

and utilizing it in the blade-pitch controller from Sec. III A. λ^{opt} is the optimal tip speed ratio corresponding to the maximum power extraction. The reference rotor speed is therefore directly related to the wind inflow velocity v that has to be estimated. The unscented Kalman filter³⁷ was utilized to estimate the wind speed, as implemented by Silva *et al.*¹⁹ Because wind speed estimators can provide uncertain information due to unmodeled effects, such as shear and induced turbulence from waked conditions, this approach can lead to deviations of the actual turbine behavior from the desired one.¹⁹ Despite uncertainties in wind speed estimation, this derating control strategy maintains a rotor speed higher than the previous strategy, which is beneficial for

power tracking as it stores more kinetic energy in the rotating components. Additionally, we saturate the reference rotor speed to the rated rotor speed $\omega_r^{\text{rated}} = 130$ rad/s. This saturation results in a decrease in the tip speed ratio when the rated rotor speed is attained during high wind speeds, such as at the above-rated condition in the baseline turbine control for power maximization. Likewise for derating control strategy I, the generator torque is set as in Eq. (15).

Figures 4 and 5 depict the gain scheduling mapping with both derating control strategies across different derating levels and wind speeds. The derating levels are denoted by the power ratios (f) ranging from 0.5 to 0.9, representing derating from 50% to 90% of the maximum power for a given wind speed. The gains change based on the current measured blade-pitch angle and rotor speed [Figs. 4(a) and 4(b)], as well as wind speed [Figs. 5(a) and 5(b)], according to Eq. (13).

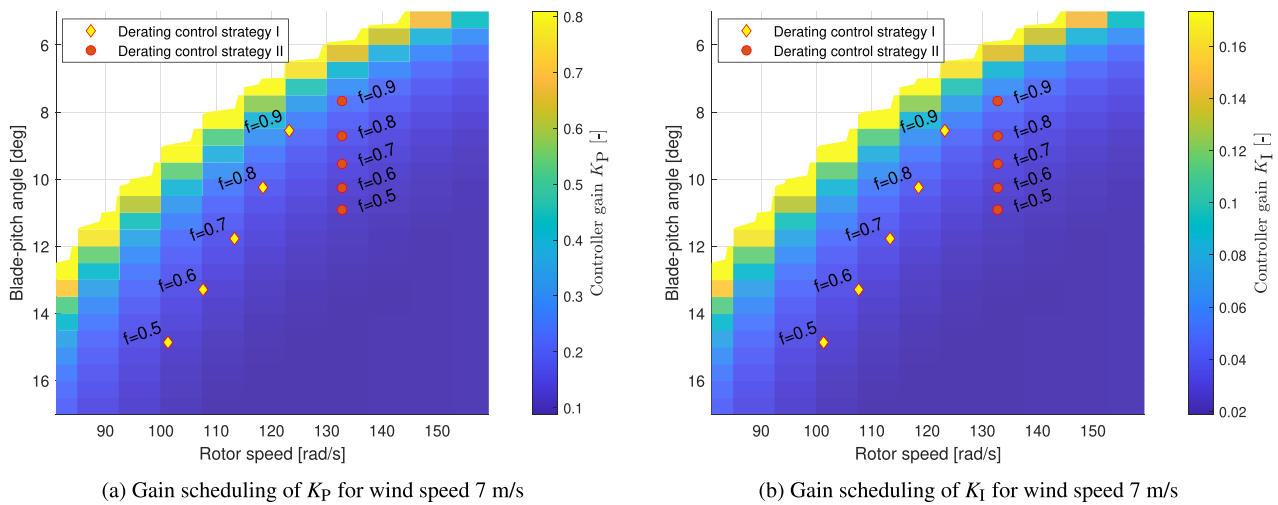
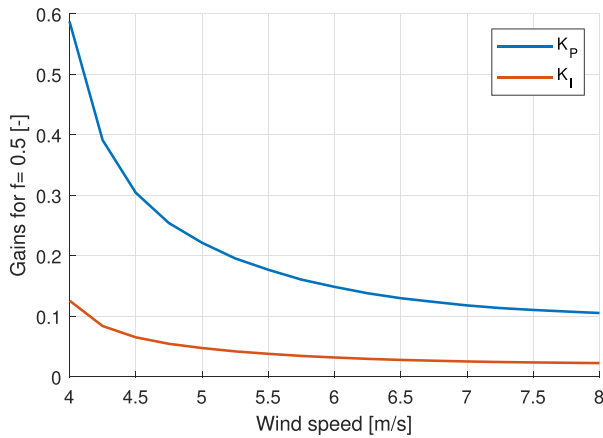
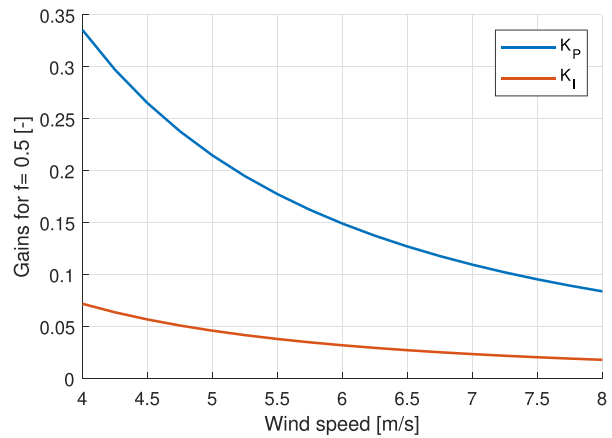


FIG. 4. PI gain scheduling of the blade-pitch control for the two derating control strategies at wind speed of $v = 7$ m/s. The derating is indicated by the power ratios ranging from $f = 0.9$ to $f = 0.5$.



(a) K_P and K_I scheduling of derating control strategy I



(b) K_P and K_I scheduling of derating control strategy II

FIG. 5. PI gain scheduling of the blade-pitch control for the two derating control strategies as a function of wind speed. The gain scheduling curves are given for a derating level of $f = 0.5$.

IV. WIND FARM CONTROL STRATEGIES

Individual wind turbines can track a specified power demand by employing the derating control strategies presented in Sec. III. However, in scenarios where wake effects are involved, such as in dense farms, notable variations in structural loading across turbines may occur, potentially resulting in an uneven lifespan for the components of the turbines. To tackle this, we suggest implementing a thrust force balance feedback to equalize aerodynamic loads throughout the farm. The aerodynamic loads serve as a proxy for structural loading in turbine components.

Additionally, as a concern related to wakes on a farm, downstream turbines may have trouble meeting their power demand due to the reduced wind availability caused by the wakes. Consequently, these downstream turbines become saturated by the available power in the wind flow as they try to keep up with demand but generate power tracking errors. To address this issue, we propose a feedback scheme

designed to compensate for these power errors. This feedback scheme is utilized for the compensation of turbine saturation resulting from wake effects.

Hence, we employ the two closed-loop wind farm controllers, previously presented in Silva *et al.*²¹ and summarized in the upcoming sections: the thrust force balance and the power compensation.

A. Thrust force balance

Figure 6 illustrates the proposed thrust force balance feedback, which employs an integral control action to achieve a balance in thrust force. The thrust force errors $e_{TB,i}^k$ of the turbine i at the discrete time index k are calculated from the mean thrust force of the M non-saturated turbines and the measured/estimated thrust force $\hat{F}_{T,i}^k$. These errors are then integrated, resulting in additional power signals $\Delta u_{TB,i}$ that are added to each power demand signal $P_{dem,i}^k$. The $N_T \times N_T$

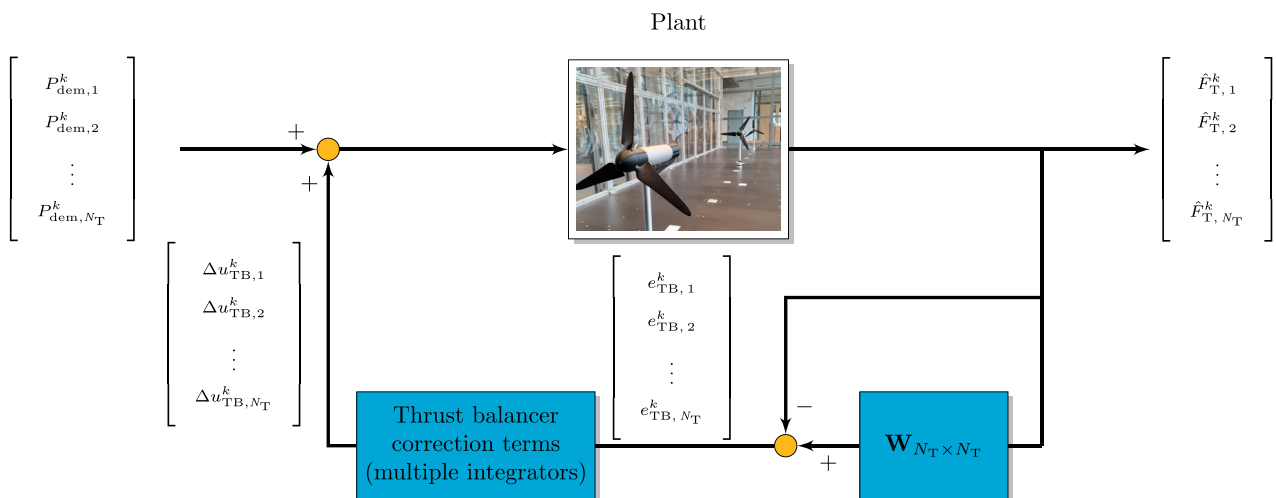


FIG. 6. Block diagram of the thrust balancer.

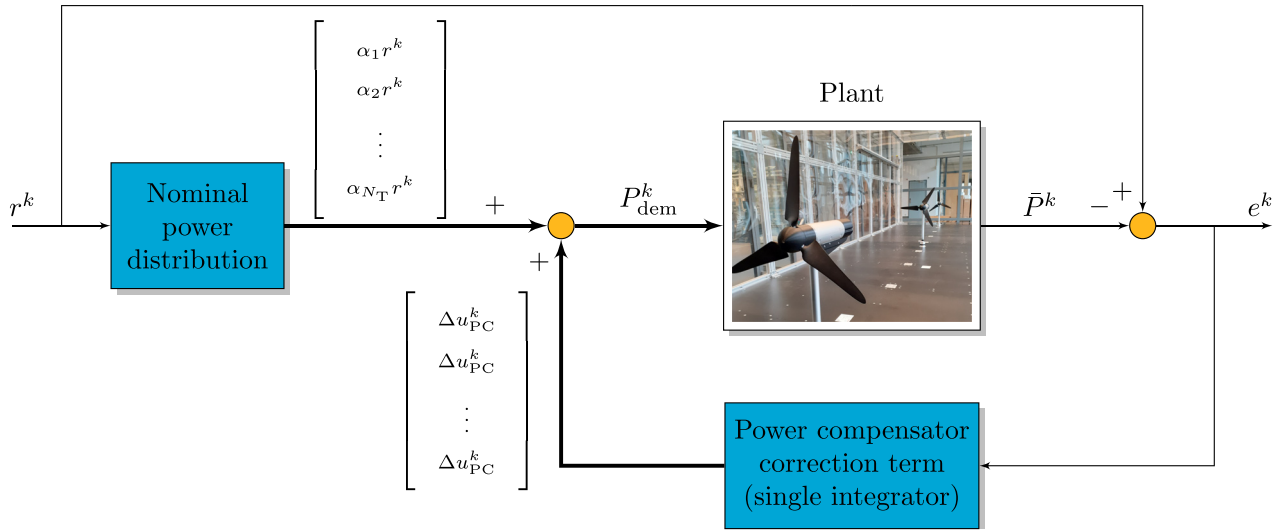


FIG. 7. Block diagram of the power compensator.

matrix \mathbf{W} aggregates the thrust force measurements for the non-saturated turbines, where N_T is the total number of turbines, and is defined as

$$\mathbf{W}_{N_T \times N_T} = [w_{ij}] = \begin{cases} 1, & \text{if } i = j \text{ is saturated,} \\ 0, & \text{if } i \neq j \text{ and } i \text{ or } j \text{ is saturated,} \\ 1/M, & \text{otherwise.} \end{cases} \quad (17)$$

The elements w_{ij} represent the individual weights of turbine $j \in 1, 2, \dots, N_T$ in the average computed for turbine $i \in 1, 2, \dots, N_T$. The vector multiplication of $\mathbf{W}_{N_T \times N_T}$ with $\hat{F}_{T,i}^k$ yields the averaged thrust forces, from which $\hat{F}_{T,i}^k$ is subtracted to determine $e_{TB,i}^k$.

In this framework, saturated turbines—those unable to meet their power demand—are excluded from the thrust force balance and their thrust force errors are zero, as defined in Eq. (17). This exclusion is important because, in cases of turbine saturation, the thrust balance feedback loop may negatively impact power tracking. As these turbines cannot generate the demanded power, the thrust force balance feedback would cause the power demand of the non-saturated turbines to decrease, while not meeting the power demand on the saturated turbines. Since saturated turbines typically experience lower aerodynamic loads, their removal is practical.

B. Power compensation

A feedback scheme, illustrated in Fig. 7, is employed to offset power mismatch within the wind farm among turbines with available resources. The power compensation feedback is composed of an integral controller to track the wind farm power demand r^k with zero steady-state power error e^k by taking the total generated power \bar{P}^k . In a feedforward manner, r^k is distributed through the use of α_i weights, in which $\sum_{i=1}^{N_T} \alpha_i = 1$. Specifically, in this work, we define $\alpha_i = 1/N_T, \forall i$. The integral controller is fed with the wind farm power error e^k , and subsequently provides the vector signal Δu_{PC}^k as output, which is added on top of the distributed power signals $\alpha_i r^k$ to define

the power demand vector P_{dem}^k . Thus, wind farm power tracking can be maintained until all turbines become saturated.

The accuracy of wind farm models can be challenging due to the complexity of atmospheric phenomena and scarce measurement information. Therefore, a pragmatic approach is considered by designing the scheme without needing a model of wind turbine interactions but the individual dynamic behavior. The common signal Δu_{PC}^k , the output of the integrator, is added in all channels ensuring that the compensation efforts are equally spread throughout the farm. This approach achieves simplicity and satisfying performance due to the timescale separation between the turbine and wake dynamics.²⁴

V. WIND TUNNEL MEASUREMENTS

In this section, we present the results obtained from the conducted experimental campaigns involving the proposed controllers. The evaluation covers the wind turbine control, spanning both individual turbine and farm scales, as well as the wind farm controllers.

A. Performance of the derating control strategies

Before delving into an analysis of the wind farm controllers, we assess the performance of the wind turbine controllers. The derating control strategy implemented at the wind turbine level defines the dynamics of power tracking and significantly influences the behavior of the wind flow within the farm. Therefore, we examine the application of the two distinct derating control strategies presented in Secs. III B and III C in different settings.

1. Single-turbine setting

To this aim, a single wind turbine was first utilized, and its responses to changes in the power reference signal have been recorded and presented in Fig. 8. The experiment involved a series of stepwise changes in the reference power, ranging from 50% to 90% of the capacity of power extraction, where the maximum power extraction at an inflow wind speed of 7 m/s would yield approximately 15 W. The

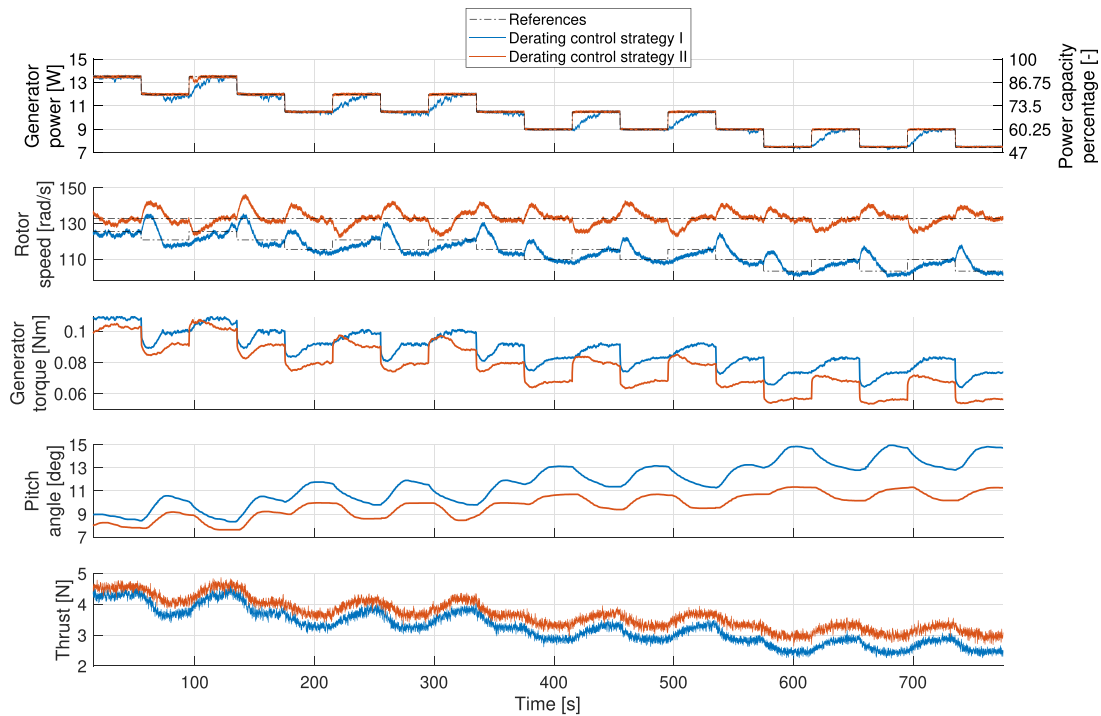


FIG. 8. Wind turbine measurements for constant inflow velocity ($v = 7$ m/s) and stepwise changes in the power reference of a single turbine.

depicted reference rotor speeds, utilized in the blade-pitch controller, were distinctly obtained according to the derating control strategies previously presented in Secs. III B and III C.

Several interesting observations can be drawn from the results depicted in Fig. 8:

- Derating control strategy I, where blade pitching is based on the greedy generator torque control law, demonstrates comparable performance with the derating control strategy II in terms of power tracking when the requested power is reduced. This is driven by the dominance of the tracking generator torque over the greedy generator torque. However, when the requested power increases, the generator torque in the derating control strategy I is constrained by the greedy generator torque. This constrained torque defaults to a more cautious, lower-value torque to prevent shutdowns caused by the low rotational speed and high generator torque values.
- Utilizing the derating control strategy II, the wind turbine demonstrated nearly flawless power tracking behavior compared to derating control strategy I. This is attributed to the higher rotor speed, which decreases the tracking generator torque below the greedy generator torque, therefore taking precedence by following the generator torque law defined in Eq. (15). However, the higher rotor speed leads to higher thrust forces compared to derating strategy I. This results in higher loads on components affected by thrust forces, such as the stresses on the base of towers.
- The tracking generator torque introduces an undesirable transient behavior in the relationship between power reference and rotor speed. This is identified analytically from Eq. (9), rewritten

in the frequency domain, such that we have the transfer function given by

$$\frac{\Delta\omega_r}{\Delta P_{ref}} = \frac{-(1/\omega_{r,0})s}{Ms^2 + Cs + K}. \quad (18)$$

The presence of a zero and a negative steady-state gain in the transfer function of Eq. (18) explain the behavior of the rotor speed in Fig. 8. This peculiarity becomes particularly noticeable during significant shifts in the power reference, as exemplified in the conducted experiment. When the power reference is lowered, the rotor speed initially increases before stabilizing. Nevertheless, in practical scenarios, the active power demand is expected to exhibit a slow-time-varying pattern, making this behavior minor. In addition, rate-limiters in the power reference signal should be considered to mitigate this effect.

- Examining the time constants, it becomes apparent that the time response of the rotor speed is longer than what was originally defined during the design [refer to Eq. (11)], approximately $\sim 40\%$ – 50% . This outcome was anticipated and stems from the considered simplifying assumptions, mainly from neglecting the damping from the greedy generator torque controller and from the variation of the aerodynamic torque with the rotor speed on the blade-pitch control design.

2. Two-turbine setting

To assess the increase in power availability at downstream turbines due to the distinct derating control strategies, we set two scaled

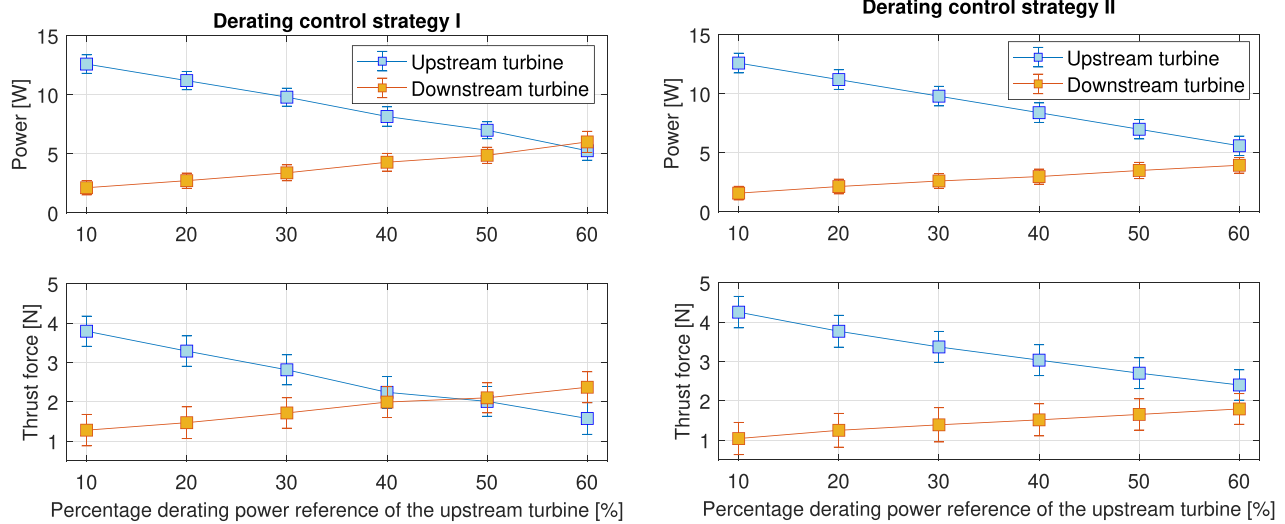


FIG. 9. Turbine power resulting from gradually derating the upstream turbine with the two derating methods in a two-turbine setting.

turbines in a full wake configuration at a free stream inflow velocity of $v = 7$ m/s. The upstream turbine is gradually derated from its greedy operation through a stepwise reduction of the power reference, while the downstream turbine always operates with greedy generator torque control and fine blade-pitch angles. The downstream turbine maximized power extraction to quantify the available power downstream. The mean and standard deviation were taken from the steady-state period after the steps in the power reference were applied in the upstream turbine. This procedure was repeated three times for each derating control strategy and the mean and standard deviation were combined.

When observing the power on the downstream turbine due to derating of the upstream turbine, the advantages of employing the derating control strategy I are noticeable (see Fig. 9). In the specific scenario when derating 50% in the power of the upstream turbine, employing the derating control strategy I leads to a mean power of 4.9 W compared to employing the derating control strategy II achieving 3.5 W. This means a 40% increase in the power obtained by the downstream turbine. This is justified by the 25.5% reduction in thrust force in the upstream turbine, moving from derating control strategy II to derating control strategy I, while generating in the upstream turbine the same amount of power. The reduction in thrust force upstream allows more energy in the flow to the downstream turbine.

However, compared to the operation with both turbines with greedy control, derating the upstream turbine by 50% in power generation results in a significant decrease in total power production, approximately 20% with derating control strategy I (see Fig. 10). Although there is an increase in power production of the downstream turbine, a reduction in total power production is observed, consistent with findings in previous numerical studies.²⁶ Nevertheless, depicted in Fig. 9, a substantial impact in structural loading is observed by derating 50% of the upstream turbine employing derating control strategy I compared to the greedy operation. This impact relates to roughly a 50% decrease in its thrust force in the upstream turbine.

3. Three-turbine setting

To further analyze the effects of the derating control strategies on the power availability in the wind farm setting, we set the three scaled turbines under full-waked conditions. We increased the inflow velocity from 7 to 8 m/s to make more energy available to the downstream turbines. During this experiment, we decreased the power request at the upstream turbine (T1) from its greedy value of around 15 W to 6 W, and set a demand of 6 W at the second turbine in the flow stream (T2). Meanwhile, the turbine furthest downstream (T3) was controlled to maximize power extraction using greedy generator torque control and fine blade-pitch angles. The power maximization of T3 is used to measure the available energy in the flow stream while applying the different derating strategies in T1 and T2.

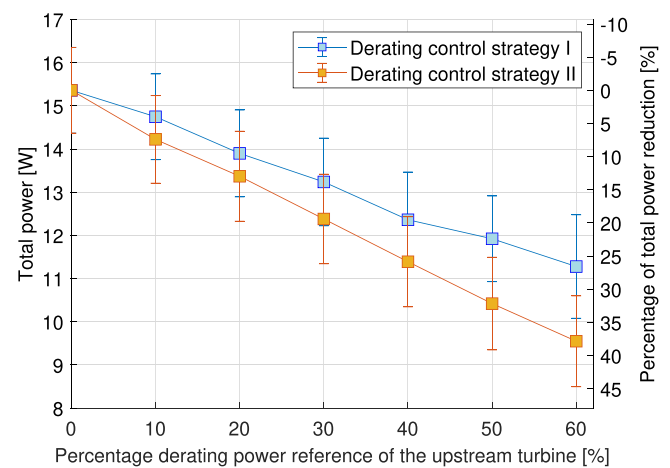


FIG. 10. Total power resulting from gradually derating the upstream turbine with the two derating methods in a two-turbine setting.

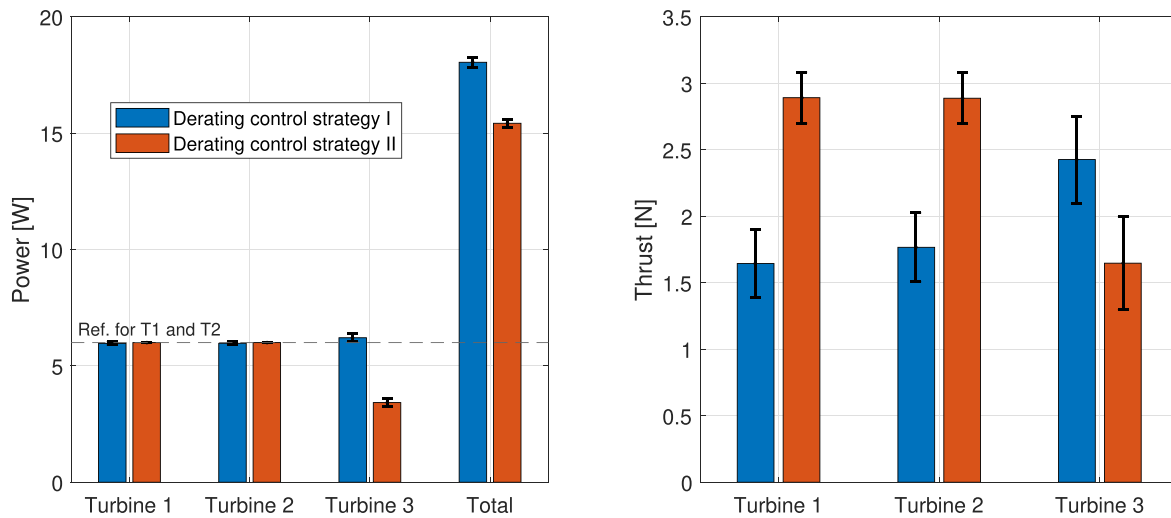


FIG. 11. Wind turbine power and thrust force results of a three-turbine setting under constant inflow velocity ($v = 8$ m/s). The power references of the two upstream turbines are set constant at $P_{dem1,2} = 6$ W.

The results illustrated in Fig. 11 show that, by reaching the power demand at both upstream turbines, the wind farm power output is 23% higher with derating control strategy I compared to derating control strategy II. The turbine T3 experiences an approximately 81% increase in its power generation. Additionally, the thrust forces are 19% and 12% lower for turbines T1 and T2, respectively. This clearly indicates the benefits of derating by blade pitching based on the greedy generator torque control compared to derating by blade pitching with constant tip speed ratio in a wind farm setting. Throughout the remainder of this paper, our attention is directed toward derating by blade pitching based on the greedy generator torque control, i.e., derating control strategy I. This focus is driven by the findings indicating its superiority regarding power capacity and structural loading.

B. Thrust force balance

In this section, we present an analysis of the fatigue loading, drawing insights from one instance of the previous open-loop wind farm results. We consider the two-turbine setting from Sec. V A 2 in two specific conditions: with greedy control in both turbines and derating the upstream turbine up to reaching thrust force balance. In the latter, the upstream turbine is derated by 50%, reducing its thrust force and allowing wind flow to the downstream turbine to achieve thrust force balance. From strain gauges placed on the bottom of each tower, the measured bending moments are utilized to estimate the fatigue loading. The procedure for estimating fatigue loading is conducted as follows:

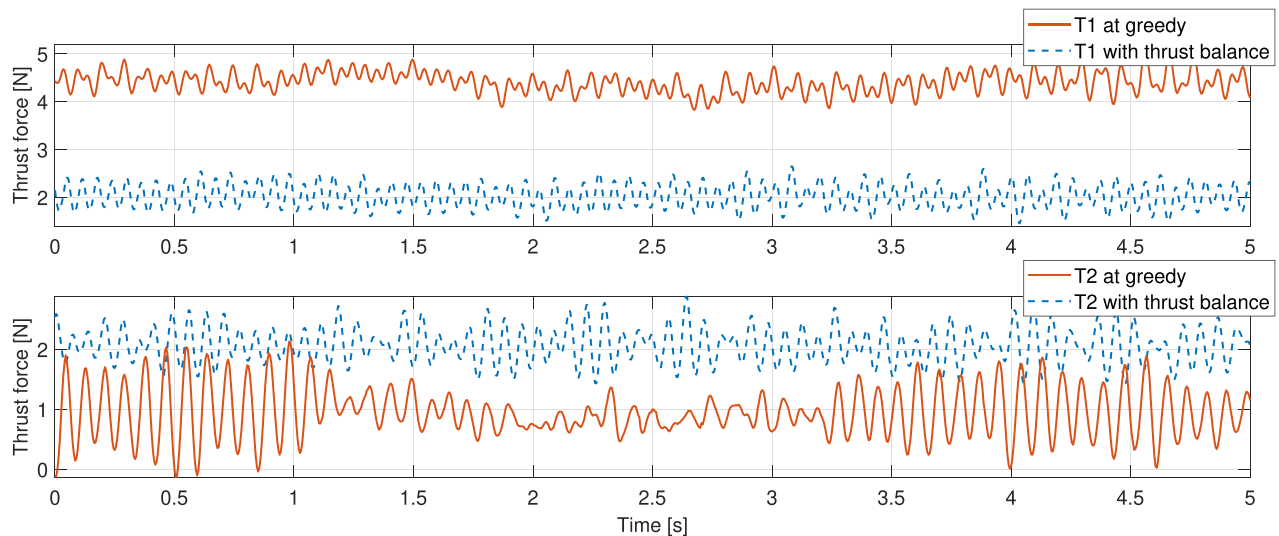


FIG. 12. Structural loading of the two turbines in greedy control operation and thrust force balance operation.

TABLE I. Fatigue loading results transitioning from greedy control to derating control strategy I reaching thrust force balance.

Derating T1 (%)	Total power (%)	Fatigue loading tower T1 (%)	Fatigue loading tower T2 (%)
50	-22.4	-4.18	-127.64

- Repeating and fluctuating stresses with non-zero mean components are counted by a rain flow counting algorithm.³⁸
- The stresses are translated to equivalent fully reversed alternating stresses.³⁹
- The fatigue damage is computed utilizing short damage equivalent load and compared between the conditions.

Fatigue loading is influenced by both the mean and the alternating stress, in which, generally, the alternating stress has a greater impact. Parts of these stress–time waveforms are shown in Fig. 12. As expected, wake effects downstream reduce mean stress while increasing alternating stress. The thrust force balance mitigates these effects downstream, while in the upstream turbine, it reduces the mean stress and might slightly increase the alternating stress. Roughly, we can see in Fig. 12 that the mean thrust force of turbine T1 reduces significantly while the alternating behavior slightly increases, resulting in a small reduction of fatigue loading at T1. On the other hand, at turbine T2, the mean value increases but, as a positive outcome, the alternating stress at the tower structure is significantly reduced. Reducing the alternating stresses in turbine T2 leads to a significant fatigue loading reduction of the tower structure.

We display the results in Table I, which demonstrate a reduction in fatigue loading not only in the derating upstream turbine T1 but mainly in turbine T2 positioned downstream. The fatigue loading calculations were conducted after the turbines had reached a steady state, determined to be 25 s after establishing the power reference setpoints.

Our estimation of fatigue loading utilized data collected over a 25-s time interval. Figure 12 displays measurements from only 5 s of this duration, focusing on visualizing the oscillation periods. Although the mean thrust force increases at T2, the result is justified by the reduction of oscillations, mainly associated with induced turbulent wake effects.

C. Balancing of aerodynamic loading in closed loop

Extending the arrangement back to three machines as depicted in Fig. 1 under full-waked conditions, we tested the proposed closed-loop controller presented in Sec. IV A. For the remainder of the paper, we employed an inflow velocity of 8 m/s. The experiments began with a low wind farm power set-point (18 W), followed by incremental increases. The goal is to identify the operational conditions that trigger turbine saturation and compare the wind farm power generation. Turbine saturation occurs when the pitch angle reaches the fine blade-pitch angle and the generator torque operates in greedy mode. In this state, the turbine maximizes power extraction, while its power demand exceeds the power being extracted.

The first experiment was carried out in an open-loop configuration, employing a uniform power distribution as our baseline, where individual power references were identical for all turbines. Figure 13 shows the time evolution of the total wind farm power, the generated power of the three wind turbines, and their thrust forces from this experiment. The thrust variation across turbines is seen as expected, along with the occurrence of turbine saturation in downstream turbines. The turbine saturation is visually noticed in Fig. 13 by the mismatch between the wind turbine power reference and its measured power output, also indicated by the vertical dashed lines.

In contrast to the data presented in Fig. 13, the results depicted in Fig. 14 illustrate the outcomes of employing the thrust balance feedback. This feedback configuration not only balances the thrust forces of non-saturated turbines but also prevents turbine saturation and enhances overall power production compared to the open-loop configuration with uniform power distribution. The thrust force balancing

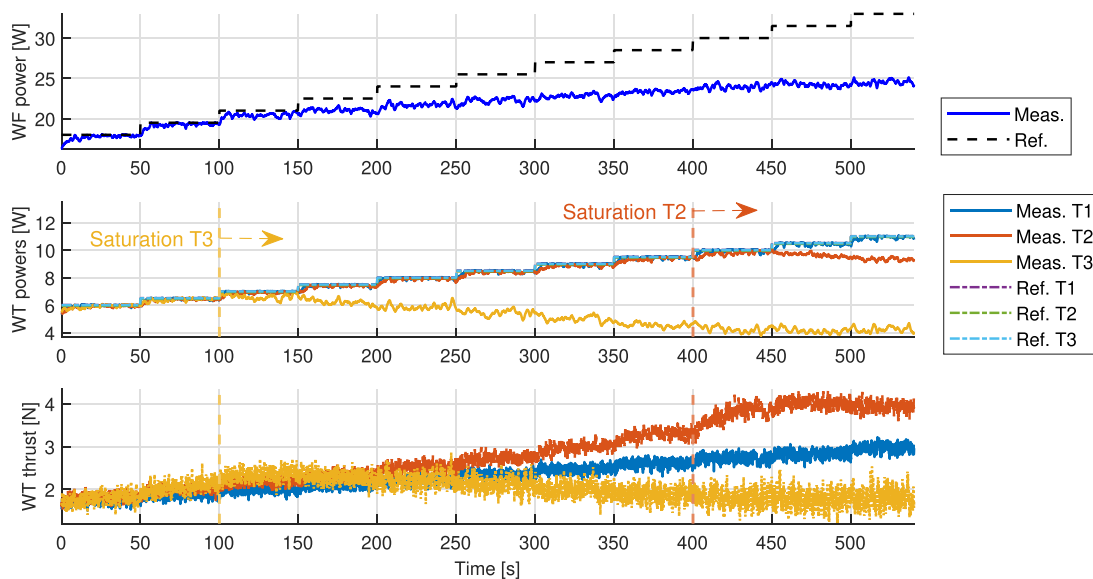


FIG. 13. Results of uniform power distribution: WF power (on the top), WT power (center), and WT thrust (on the bottom). In the WT power plot, all references are identical.

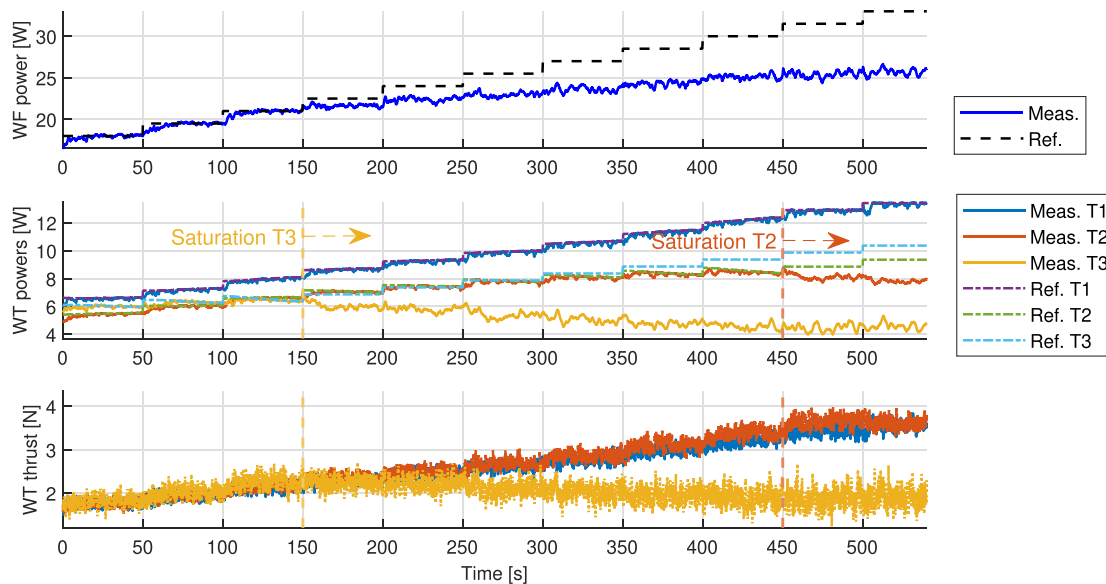


FIG. 14. Results of thrust force balancing: WF power (on the top), WT power (center), and WT thrust (on the bottom).

leads to an increase in wind farm power of approximately 3%–5% observed between 450 and 500 s. This is attributed to the increase in power availability in downstream turbines, a result that is in line with what was reported utilizing simulations by Silva *et al.*²⁵ The prevention of turbine saturation is evident when comparing Figs. 13 and Fig. 14.

As discussed in Sec. IV A, when a turbine saturates, it is excluded from the thrust balance controller, resulting in a noticeable disparity in the thrust forces between saturated and unsaturated turbines. This measure was adopted to avoid conflicting behavior with power generation. Saturated turbines, unable to meet their power demand, typically have lower thrust forces. If the saturated turbine is not excluded, it would decrease the power demand on unsaturated turbines through the thrust force balance feedback. Consequently, this would create a gap in the total power production since saturated turbines cannot generate their counterparts. However, by removing saturated turbines from thrust force balancing, total power generation remains unaffected by turbine saturation, while their thrust forces are generally lower than those still undergoing balancing.

D. Compensation of wake power losses in closed loop

Increasing the reliability of energy production in wind farms is considered an important research challenge.⁴⁰ In the results, we show that energy production can be enhanced by wind farm control. With the proposed power compensator from Sec. IV B, although the growth of the total power demand triggers turbine saturation, the energy losses can be redistributed and harvested by the turbines that are still capable of generating additional power.

The measurements shown in Fig. 15 make it clear that the closed-loop approach for power compensation leverages the wind farm power tracking capability. The thrust balance controller was not applied during these measurements. Focusing on the total wind farm power illustrated in the top subplots, we observe that the offset in the wind farm power in the two previous experiments is significantly reduced, such

that the wind farm power output better agrees with its increasing reference. The power losses were compensated with the implementation of the power compensation feedback. Despite the occurrence of turbine saturation in T3 and T2, respectively, the wind farm power set-point could still be maintained for up to 350 s at 27 W, as opposed to 22 W in 150 s observed in Fig. 14. Beyond 400 s, all turbines reached saturation, and the escalating power demand could not be met.

Sustaining the power tracking comes at the expense of heightened load variability across the turbines. We combine the two control strategies to mitigate this effect while the thrust force balancing does not influence power compensation. The results are depicted in Fig. 16 and demonstrate power compensation while balancing the thrust forces of the non-saturated turbines. However, the thrust force difference across turbines is still significant because the thrust balance is limited to unsaturated turbines. Nevertheless, in the first steps of the experiment, it has a positive effect by spreading the structural loads and avoiding saturation without compromising the power tracking capability.

VI. CONCLUSIONS

This work introduced a blade-pitch controller designed for derating control strategies. Subsequently, derating control strategies were proposed and assessed for their distinct impacts, taking into account not only individual turbine performance but also their influence on downstream turbines. After selecting the derating control strategy aimed at mitigating loading and enhancing the farm's available power, we conducted the experiments with the closed-loop control structures that effectively balanced thrust forces and compensated for power losses due to wake effects.

The experimental findings reveal promising avenues for the implementation of active power controllers in wind farms. The closed-loop blade-pitch control derived for derating control strategies provides precise target power output and rotor speed, in contrast to open-

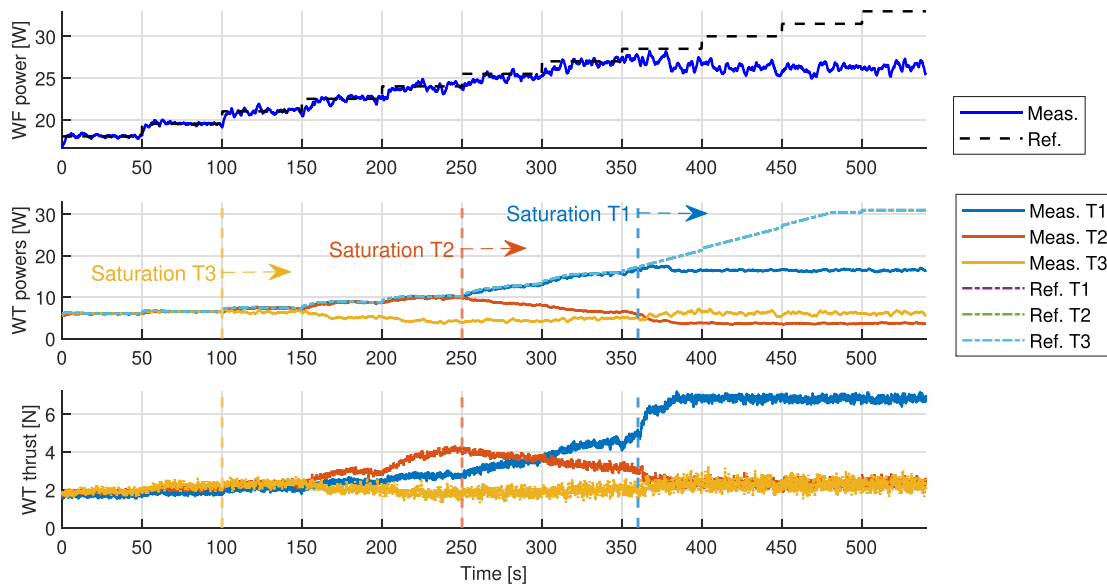


FIG. 15. Results of power compensation: WF power (on the top), WT power (center), and WT thrust (on the bottom). In the WT power plot, all references are identical.

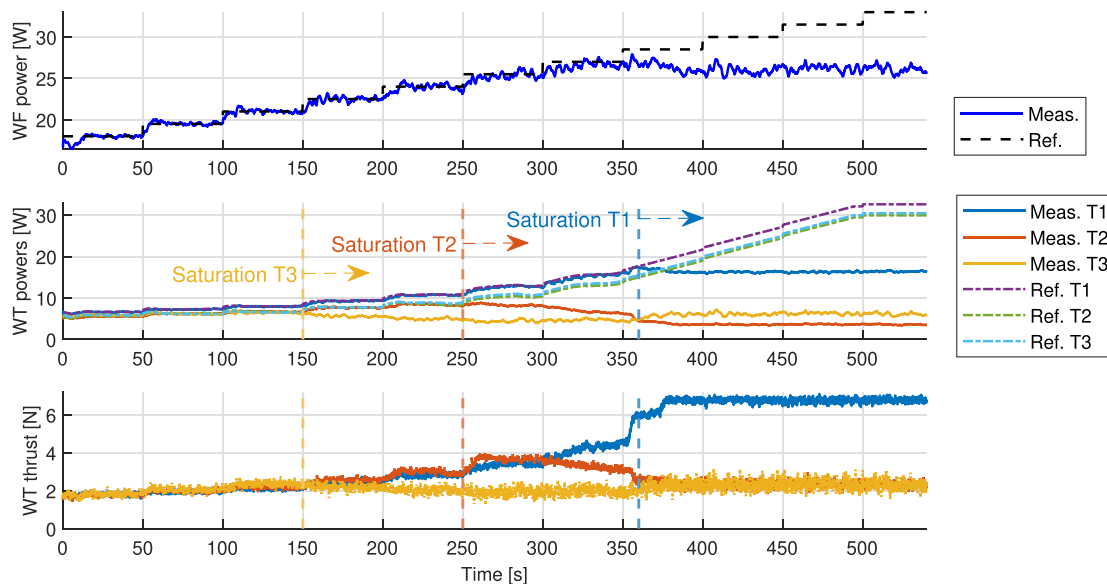


FIG. 16. Results of power compensation and thrust force balancing: WF power (on the top), WT power (center), and WT thrust (on the bottom).

loop approaches that make use of lookup tables. Notably, the performance of the wind farm is directly associated with the adopted derating control strategy. The derating control strategy based on the greedy generator torque control, although having a slower response in the power tracking, favors the wind farm's total power production compared to the strategy with constant tip speed ratio. In the two-turbine case, the power capacity downstream showed an increase of approximately 40%, whereas in the three-turbine case, the power capacity increase at the third turbine reached about 81%. Furthermore, derating

the upstream turbines exhibits significant reductions in thrust force and fatigue loading on the tower structure, albeit at the expense of a decrease in the total power generation when transitioning from greedy farm operation to a thrust force balancing condition in a full-waked scenario. Moving from maximizing power generation to on-demand power generation, thrust force balancing remains a potential strategy by anticipating requests for low power levels. Still, the thrust force balancing shall be implemented only in the non-saturated turbines not affecting the wind farm power generation.

In the evaluation of the proposed wind farm controllers, three different approaches were considered: an open-loop configuration with uniform power distribution; a closed-loop controller for balancing thrust forces; and a closed-loop controller for power compensation. Achieving thrust force balance in the non-saturated turbines, the closed-loop controller for balancing thrust forces avoids turbine saturation and enhances the total power capacity compared to the uniform power distribution in approximately 3%–5%. Furthermore, the application of power compensation significantly enhances power tracking by eliminating power errors caused by turbine saturation. This results in meeting the upper limit power demand of 27 W, compared to 22 W from the other two approaches, reflecting a 22% boost in power tracking capability.

The results of power gains and fatigue loading reduction in this paper hold for the specific experimental setting. The reduction in fatigue loading is computed based on the specific structure geometry and material properties of the scaled turbines. To extrapolate these results to multi-megawatt wind turbines, a comprehensive analysis must be conducted accordingly, along with non-scaled experimental campaigns. Nonetheless, the same trends are expected in the context of large-scale turbines, with these findings positively contributing to enhancing wind farm control strategies and advancing research efforts further.

ACKNOWLEDGMENTS

The authors would like to acknowledge the financial support provided by WATEREYE, a project funded by the European Union Horizon 2020 research and innovation program (Grant No. 851207) under the call H2020-LC-SC3-2019-RES-TwoStages. Additionally, we would like to acknowledge the technical support of Ralph J. M. Willekes, Will J. M. van Geest, and Wim H. A. Wien from TU Delft and contributions from Bert Van den Abbeele in setting the experiments.

AUTHOR DECLARATIONS

Conflict of Interest

The authors have no conflicts to disclose.

Author Contributions

J. Gonzalez Silva: Conceptualization (lead); Data curation (equal); Formal analysis (lead); Investigation (equal); Methodology (lead); Software (equal); Validation (equal); Visualization (equal); Writing – original draft (lead); Writing – review & editing (equal). **D. van der Hoek:** Conceptualization (equal); Data curation (equal); Formal analysis (equal); Investigation (equal); Methodology (equal); Software (equal); Validation (equal); Visualization (equal); Writing – review & editing (equal). **R. Ferrari:** Conceptualization (equal); Funding acquisition (equal); Project administration (equal); Resources (equal); Supervision (equal); Writing – review & editing (equal). **J. W. van Wingerden:** Conceptualization (equal); Funding acquisition (equal); Project administration (equal); Resources (equal); Supervision (equal); Writing – review & editing (equal).

DATA AVAILABILITY

The data that support the findings of this study are available from the corresponding author upon reasonable request.

REFERENCES

- 1P. Fleming, J. Aho, P. Gebraad, L. Pao, and Y. Zhang, “Computational fluid dynamics simulation study of active power control in wind plants,” Report No. NREL/CP-5000-66004 (National Renewable Energy Laboratory, 2016).
- 2S. Boersma, B. M. Doekemeijer, P. M. O. Gebraad, P. A. Fleming, J. Annoni, A. K. Scholbrock, J. A. Frederik, and J. W. van Wingerden, “A tutorial on control-oriented modeling and control of wind farms,” in *American Control Conf. (ACC)* (IEEE, 2017).
- 3J. A. Frederik, R. Weber, S. Cacciola, F. Campagnolo, A. Croce, C. Bottasso, and J.-W. van Wingerden, “Periodic dynamic induction control of wind farms: Proving the potential in simulations and wind tunnel experiments,” *Wind Energy Sci.* **5**, 245–257 (2020).
- 4F. Díaz-González, M. Hau, A. Sumper, and O. Gomis-Bellmunt, “Participation of wind power plants in system frequency control: Review of grid code requirements and control methods,” *Renewable Sustainable Energy Rev.* **34**, 551–564 (2014).
- 5E. Ela, V. Gevorgian, P. A. Fleming, Y. C. Zhang, M. Singh, E. Muljadi, A. Scholbrock, J. Aho, A. Bucksman, L. Y. Pao, V. Singhvi, A. Tuohy, P. Pourbeik, D. Brooks, and N. Bhatt, “Active power controls from wind power: Bridging the gaps,” Report No. NREL/TP-5D00-60574 (National Renewable Energy Laboratory, 2014).
- 6T. Eguinoa, T. Göçmen, P. B. Garcia-Rosa, K. Das, V. Petrović, K. Kölle, A. Manjock, M. J. Koivisto, and M. Smailes, “Wind farm flow control oriented to electricity markets and grid integration: Initial perspective analysis,” *Adv. Control Appl.* **3**, e80 (2021).
- 7P. Veers *et al.*, “Grand challenges in the science of wind energy,” *Science* **366**, eaau2027 (2019).
- 8WindEurope, “Future system needs and the role of grid-forming converters,” Wind Europe position papers (2019), <https://windeurope.org/policy/position-papers/future-system-needs-and-role-of-grid-forming-converters/> (accessed 2023-09-12).
- 9J. Morales, A. Conejo, H. Madsen, P. Pinson, and M. Zugno, *Integrating Renewables in Electricity Markets: Operational Problems*, International Series in Operations Research and Management Science (Springer US, 2013).
- 10E. Castronuovo and J. Lopes, “On the optimization of the daily operation of a wind-hydro power plant,” *IEEE Trans. Power Syst.* **19**, 1599–1606 (2004).
- 11L. Bird, D. Lew, M. Milligan, E. M. Carlini, A. Estanqueiro, D. Flynn, E. Gomez-Lazaro, H. Holttinen, N. Menemenlis, A. Orth, P. B. Eriksen, J. C. Smith, L. Soder, P. Sorensen, A. Altiparmakis, Y. Yasuda, and J. Miller, “Wind and solar energy curtailment: A review of international experience,” *Renewable Sustainable Energy Rev.* **65**, 577–586 (2016).
- 12J. Jenkins, Z. Zhou, R. Ponciroli, R. Vilim, F. Ganda, F. de Sisternes, and A. Botterud, “The benefits of nuclear flexibility in power system operations with renewable energy,” *Appl. Energy* **222**, 872–884 (2018).
- 13ENTSO-E, “ENTSO-E network code for requirements for grid connection applicable to all generators” (2016), https://www.entsoe.eu/network_codes/ (accessed 2022-08-17).
- 14J. Aho, P. Fleming, and L. Y. Pao, “Active power control of wind turbines for ancillary services: A comparison of pitch and torque control methodologies,” in *American Control Conference (ACC)* (IEEE, 2016), pp. 1407–1412.
- 15D. van der Hoek, S. Kanev, and W. Engels, “Comparison of down-regulation strategies for wind farm control and their effects on fatigue loads,” in *Annual American Control Conference (ACC)* (IEEE, 2018), pp. 3116–3121.
- 16W. H. Lio, M. Mirzaei, and G. C. Larsen, “On wind turbine down-regulation control strategies and rotor speed set-point,” *J. Phys.: Conf. Ser.* **1037**, 032040 (2018).
- 17K. Ma, J. Zhu, M. Soltani, A. Hajizadeh, and Z. Chen, “Wind turbine down-regulation strategy for minimum wake deficit,” in *11th Asian Control Conference (ASCC)* (IEEE Press, 2017), pp. 2652–2656.
- 18K. Kim, H. Kim, C. Kim, I. Paek, C. Bottasso, and F. Campagnolo, “Design and validation of demanded power point tracking control algorithm of wind turbine,” *Int. J. Precis. Eng. Manuf.-Green Technol.* **5**, 387–400 (2018).
- 19J. G. Silva, Y. Liu, R. Ferrari, and J.-W. van Wingerden, “UKF-based wind estimation and sub-optimal turbine control under waked conditions,” *IFAC-PapersOnLine* **56(2)**, 7662–7667 (2023).

- ²⁰M. Vali, V. Petrović, G. Steinfeld, L. Y. Pao, and M. Kühn, “An active power control approach for wake-induced load alleviation in a fully developed wind farm boundary layer,” *Wind Energy Sci.* **4**, 139–161 (2019).
- ²¹J. G. Silva, R. Ferrari, and J.-W. van Wingerden, “Wind farm control for wake-loss compensation, thrust balancing and load-limiting of turbines,” *Renewable Energy* **203**, 421–433 (2023).
- ²²S. J. Price and R. B. Figueira, “Corrosion protection systems and fatigue corrosion in offshore wind structures: Current status and future perspectives,” *Coatings* **7**, 25 (2017).
- ²³T. Knudsen, T. Bak, and M. Svenstrup, “Survey of wind farm control–power and fatigue optimization,” *Wind Energy* **18**, 1333–1351 (2015).
- ²⁴J. W. van Wingerden, L. Pao, J. Aho, and P. Fleming, “Active power control of waked wind farms,” *IFAC-PapersOnLine* **50**, 4484–4491 (2017).
- ²⁵J. G. Silva, B. Doekemeijer, R. Ferrari, and J.-W. van Wingerden, “Active power control of waked wind farms: Compensation of turbine saturation and thrust force balance,” in *European Control Conference (ECC)* (IEEE, 2021) pp. 1223–1228.
- ²⁶J. Annoni, P. M. O. Gebraad, A. K. Scholbrock, P. A. Fleming, and J.-W. van Wingerden, “Analysis of axial-induction-based wind plant control using an engineering and a high-order wind plant model,” *Wind Energy* **19**, 1135–1150 (2016).
- ²⁷D. van der Hoek, S. Kanev, J. Allin, D. Bieniek, and N. Mittelmeier, “Effects of axial induction control on wind farm energy production—A field test,” *Renewable Energy* **140**, 994–1003 (2019).
- ²⁸F. Campagnolo, V. Petrović, J. Schreiber, E. M. Nanos, A. Croce, and C. L. Bottasso, “Wind tunnel testing of a closed-loop wake deflection controller for wind farm power maximization,” *J. Phys.: Conf. Ser.* **753**, 032006 (2016).
- ²⁹V. Petrović, J. Schottler, I. Neunber, M. Hölling, and M. Kühn, “Wind tunnel validation of a closed loop active power control for wind farms,” *J. Phys.: Conf. Ser.* **1037**, 032020 (2018).
- ³⁰F. Noca, G. Catry, N. Bosson, L. Bardazzi, S. Marquez, and A. Gros, “Wind and weather facility for testing free-flying drones,” AIAA Paper No. AIAA 2019-2861, 2019.
- ³¹J. Schottler, A. Hölling, J. Peinke, and M. Hölling, “Design and implementation of a controllable model wind turbine for experimental studies,” *J. Phys.: Conf. Ser.* **753**, 072030 (2016).
- ³²P. Å. Krogstad and P. E. Eriksen, “Blind test’ calculations of the performance and wake development for a model wind turbine,” *Renewable Energy* **50**, 325–333 (2013).
- ³³A. van Vondelen, D. van der Hoek, S. Navalkar, and J. van Wingerden, “Synchronized dynamic induction control: An experimental investigation,” *J. Phys.: Conf. Ser.* **2767**, 032027 (2024).
- ³⁴M. Hansen, A. Hansen, T. Larsen, S. Øye, P. Sørensen, and P. Fuglsang, “Control design for a pitch-regulated, variable speed wind turbine,” Technical Report No. 1500 (Forskningscenter Risø, 2005).
- ³⁵J. Jonkman, S. Butterfield, W. Musial, and G. Scott, “Definition of a 5-MW reference wind turbine for offshore system development,” Report No. NREL/TP-500-38060 (National Renewable Energy Laboratory, 2009).
- ³⁶J. G. Silva, D. van der Hoek, S. P. Mulders, R. Ferrari, and J.-W. van Wingerden, “A switching thrust tracking controller for load constrained wind turbines,” in *American Control Conference (ACC)* (IEEE, 2022), pp. 4230–4235.
- ³⁷S. J. Julier, J. K. Uhlmann, and H. F. Durrant-Whyte, “A new approach for filtering nonlinear systems,” in *American Control Conference* (IEEE, 1995), Vol. 3, pp. 1628–1632.
- ³⁸ASTM International, “Standard practices for cycle counting in fatigue analysis,” Standard No. ASTM E1049-85 (ASTM International, 2017).
- ³⁹R. Budynas and K. Nisbett, *Shigley’s Mechanical Engineering Design*, 11th ed. (McGraw-Hill Higher Education, 2020).
- ⁴⁰J. W. van Wingerden, P. A. Fleming, T. Göçmen, I. Eguinoa, B. M. Doekemeijer, K. Dykes, M. Lawson, E. Simley, J. King, D. Astrain, M. Iribas, C. L. Bottasso, J. Meyers, S. Raach, K. Kölle, and G. Giebel, “Expert elicitation on wind farm control,” *J. Phys.: Conf. Ser.* **1618**, 022025 (2020).